Wide Field of View (FOV) Imagers for Co-Orbiting Object Detection

Randa Qashoa
York University
Paul Harrison
Magellan Aerospace
Regina S.K Lee
York University

ABSTRACT

Space-based optical systems are powerful tools for providing Space Situational Awareness (SSA) and Space Domain Awareness (SDA) as they are not limited by weather or by fixed geographic location. As part of Canada's new microsatellite SDA mission, named Redwing, a wide field imaging capability will be employed for both proximity and co-orbital awareness around Redwing's Low Earth Orbit (LEO). Repeated close-range observations of "co-orbiting" objects are highly valuable for accurate orbit determination, as well as assessment of collision risk for the host platform. Co-orbiting objects present a geometric challenge in observation, however, in that the look angles can vary rapidly during close approaches [1]. In addition to co-orbital objects, the increasing congestion in LEO is giving rise to many objects in near-coplanar orbits of different altitudes. A method to survey coplanar and co-orbital space objects is somewhat underdeveloped and observability issues are weakly addressed. As many optical space surveillance sensors' targets are often viewed at ranges greater than 1000 km, a technology and concept of operations gap exists when performing space surveillance on objects at ranges less than 250 km from the host sensor in space.

A variety of different imaging options are utilized for Resident Space Object (RSO) detection. To have an awareness of as many RSOs near the host platform as possible, as opposed to having a more detailed view of a smaller portion of the sky, wide Field-Of-View (FOV) systems are used. These can be dedicated sensors for RSO detection, or they could be sensors developed for other purposes, such as star trackers that are used in a dual-purpose fashion. Even though wide-FOV sensors tend to have smaller apertures and therefore do not have the faint magnitude detection capability of large-aperture / narrow-FOV systems, the ability to study larger volumes of nearby sky is highly desirable for the co-orbital tracking application. There are in fact many examples of using wide FOV systems for SSA, including projects that the authors have previously participated in. For example, in [2] the Cascade, Smallsat and Ionospheric Polar Explorer's (CASSIOPE's) Fast Auroral Imager (FAI) has been used for RSO detection, while in [3], the PCO Panda 4.2 and the UI-3370CP-M-GL IDS were used to capture starfield images from a stratospheric balloon platform at about 40 km in altitude.

The goal of this study is to compare different small-aperture / wide-FOV sensors by assessing their RSO detection limits. This includes finding the number of detectable co-orbiting RSOs that regularly pass within 250 km of the observer, the expected brightness of detected RSOs, as well as other supporting statistics. When designing an SSA mission, choosing the correct sensor is a challenging task but one with important consequences on achieving mission goals. By comparing the performance of different sensors in RSO detection performance, we can determine which sensors would best accomplish mission objectives.

To perform this analysis, an algorithm was developed to model the orbit of the observing platform along with orbits of potential nearby RSOs in the sky around it. Then the brightness and signal-to-noise ratio (SNR) for different sensors are calculated to determine the detection capabilities for these sensors. For this study, a comparison between three sensors is made. The sensors chosen for the comparison are the FAI, the PCO Panda 4.2, and UI-3370CP-M-GL IDS cameras. All three of these sensors have been used for SSA purposes in previous research, and have well-established optical characteristics, which make them ideal candidates for this study. A crucial extension to this, which is examined at a preliminary level, is the use of repeat observations by these wide-FOV sensors during close approaches to obtain useful orbit knowledge.

This analysis is being performed with an eye to using low-cost, off-the-shelf, and dual-purposed sensors to provide SSA across multiple distributed platforms, including non-SSA missions. The authors are performing proximity analysis for the Redwing mission, so this research is being applied to dedicated SSA/SDA mission development as well as being a general sensor trade study.

Table 1: Sensor parameter comparison between the FAI, PCO, & IDS cameras.

Sensor Name	Resolution	Pixel Pitch (µm)	Focal Length (m)	FOV (degrees)	Average Angular Resolution Per Pixel (deg/pixel)	Aperture Diameter (mm)
FAI	256 x 256	26	0.0136	26	0.102	17.25
PCO Panda 4.2	2048 x 2048	6.5	0.025	29.6	0.014	57
UI-3370CP-M-GL IDS	2048 x 2048	5.5	0.016	41	0.02	15.93

1. INTRODUCTION

Within the space community, there has recently been a growing interest in the fields of Space Situational Awareness (SSA) & Space Domain Awareness (SDA). SSA & SDA focus on understanding Resident Space Objects (RSOs), such as satellites, rocket bodies, and debris that are orbiting the Earth by detecting, tracking, and identifying the RSOs orbiting near our satellites of interest. There are many different approaches to tackle SSA & SDA and one of the most promising ones is developing SSA satelllites with optical systems. In our previous studies, we determined the feasibility of using low resolution wide Field-Of-View (FOV) sensors, such as star trackers, for RSO detection. As a technology demonstration for a future SSA mission, we launched two payloads on stratospheric balloons in 2022 and 2023 to test the capability of different cameras for RSO detection. As demonstrated in [3], the UI-3370CP-M-GL IDS & the PCO Panda 4.2 (in [3, 4]) were able to successfully capture RSOs under near-space observation environments. Additionally, in [2], we demonstrated the use of the Fast Auroral Imager (FAI) which is a sensor onboard the Cascade, Smallsat and Ionospheric Polar Explorer (CASSIOPE) for RSO detection. Given that we verified that all three sensors are capable of capturing RSOs, we chose these sensors for the analysis presented in this study. The main sensor parameters for the FAI, PCO, & IDS cameras are provided in Table 1.

When designing a space mission, selecting the appropriate payload to mission objectives is of great importance. When it comes to SSA missions where the main function of the optical sensor is to capture as many nearby RSOs as possible, it becomes difficult to assess which sensor would be sufficient for the mission. Most star tracker datasheets do not provide information about signal-to-noise ratio (SNR) and visual magnitude detectability limits of different sensors. As a result, there is a need to properly analyze the available parameters of different SSA sensors to determine the capability of each sensor in co-orbiting RSO detection. This study demonstrates a detectability analysis that is used to compare and determine the capabilities of the FAI, PCO, & IDS cameras to observe nearby co-orbiting objects. We are currently working on Canada's next generation SSA mission, named Redwing, and are implementing a similar analysis for selecting the appropriate hardware for the mission. We are currently working on Canada's next generation SSA mission, named Redwing, and are implementing a similar analysis for selecting the appropriate hardware for the mission.

2. METHODOLOGY

In this section, we explore the parameters used in defining the study as well as an explanation of the SNR calculation needed to determine the detectability of objects.

2.1 Study Parameters

For this analysis, multiple parameters are defined that are adjusted to accommodate different mission scenarios. Firstly, the orbit of the host or observer RSO is defined. In this study, we are using CASSIOPE's orbital parameters on March 21, 2023 as obtained by its Two-Line Elements (TLEs). In this study, as well as the Redwing microsatellite mission, we are focusing on co-orbiting objects given the challenge in observing them due to the quickly changing look angles as explained in [1]. The orbital parameters for the host as well as the variation range of each parameter for a co-orbiting object are provided in Table 2. The parameters were varied according to a normal distribution.

Table 2: Host & target orbital parameters.

Orbit Element	Host (CASSIOPE) Orbit	Variation Relative To Host
Semimajor Axis	7115.7 km	± 100 km
Eccentricity	0.0584161	≤ 0.015
Inclination	80.9642°	± 1°
RAAN	332.1°	±3°
Argument of Perigee	213.1°	0° to 360°
True Anomaly	147.7°	0° to 360°

When performing alternative studies, the amount of variation to define a co-orbiting object does not need to be adjusted unless the host orbit has a large eccentricity. The only change would be in the host orbital parameters. Following the orbital parameters, the other parameters that impact the study are the duration of the study window, the threshold distance to assign an RSO as a co-orbiting object, the SNR threshold for detectability, & the diameter of the target object. The values of these parameters that are utilized in this study are in Table 3.

Table 3: List of detectability analysis parameters.

Analysis Parameters	Value
Orbit propagation duration	1 day
Number of generated targets	100
Maximum host to target distance	250 km
Minimum SNR	6
Diameter of target RSO	20 cm

As per Table 3, the orbit of the host and the surrounding targets are propagated for 1 day. While using the orbital parameter range in Table 2 generates co-orbiting objects, this study focuses on very close approaching targets within 250 km of the observer RSO. This threshold was chosen to focus this study on nearby object surveillance. Given that we are looking for the detectability limits of each sensor, the study focuses on small 20 cm diameter targets such as debris and cubesats. A minimum SNR of 6 allows us to ensure a true detection. All these parameters are interchangeable for future mission studies where the analysis requirements differ from this study.

2.2 Determining Sensor Detectability

This section explains the steps taken to determine the number of detected objects for each sensor. The first step is to calculate the position vector for Redwing using the orbital parameters in Table 2 for the full propagation duration, which is set to 1 day in this study. The next step is to generate the orbits for the 100 surrounding targets. A normal distribution is implemented where the mean is the original host's orbital parameters and the standard deviation is the variation relative to host as per Table 2. The only exceptions to this are the argument of perigee and the true anomaly which are randomly assigned values between 0 and 360 degrees. Using the co-orbiting orbital parameters, a set of position vectors are generated for each of the 100 targets. Following that, the host to target distance is calculated and all objects further than 250 km are excluded from the rest of the study. The list of target position vectors and distances to host spacecraft is then saved to ensure consistency when testing the different sensor parameters.

With the orbital information known, the detectability analysis can be performed. There are two different analyses performed. The first analysis is to determine the impact of integration time on the number of detected RSOs from the selected sensors: FAI, PCO, & IDS. The second, more detailed analysis focuses on the value of object visual magnitude and SNR at the target RSO's entry, exit, minimum rate, and minimum distance points. Regardless of which analysis is performed, the main values to calculate are the visual magnitude and SNR. Equations 1 - 3 are used to calculate the visual magnitude.

$$\Phi = \pi - cos^{-1}([TargetPosition_{ECI} - HostPosition_{ECI}] \cdot Sun_{ECI}) \tag{1}$$

$$F(\Phi) = \left(\frac{2}{3\pi^2}\right)[(\pi - \Phi)cos\Phi + sin\Phi] \tag{2}$$

$$m_{obj} = m_{sun} - 2.5log\left(\frac{\rho A_{target} F(\Phi)}{R^2}\right) \tag{3}$$

In Equations 1 - 3, Φ is the solar phase angle which is the sun-target-host RSO angle. The phase angle is calculated using the dot product of the target position as measured from the observer in the ECI frame and the sun's ECI position vector. $F(\Phi)$ is a function relating illumination phase angle to fraction of light reflected. This function is typically a combination of specular and diffuse reflection. In this study, the RSOs are assumed to be spheres and we only assume diffuse reflection which results in Equation 2 from [5]. A spherical object also encounters specular reflection, but in this case, the amount is negligible so only the diffuse reflection is considered in this study. m_{obj} is the visual magnitude of the target and m_{sun} is the visual magnitude of the sun which is -26.74. ρ is the target RSO's diffuse reflectivity which is assumed to be 0.2 in this study. A_{target} is the area of the target which is $\frac{\pi d_{target}^2}{4}$ for a spherical object where d_{target} is the target RSO's diameter. Lastly, R is the range or the distance between the target and the RSO.

Using the visual magnitude, the number of signal photoelectrons are calculated using the equations presented in [6] which are reproduced in Equations 4 & 5.

$$E_{RSO} = 5.6 \times 10^{10} \times 10^{-0.4 m_{obj}} \tag{4}$$

$$e_s = Q_e \times \tau \times A \times E_{rso} \times t_{signal} \tag{5}$$

In Equations 4 & 5, E_{RSO} is the photon irradiance in $ph/s/m^2$, Q_e is the sensor's quantum efficiency, τ is the optical transmittance, A is the aperture area which is calculated as $\frac{\pi D_{aperture}^2}{4}$. The equation for signal provided in [6] also adds an atmospheric transmittance factor but this is assigned to be 1 in this study since we are assessing a space-based observer as opposed to a ground-based observer. t_{signal} refers to the signal integration time which has a maximum value equal to the sensor's selected integration time. In practice, integration time is usually less than this maximum value as a target with an angular rate relative to the sensor will be within the sensor's FOV for a limited period. The system integration time is calculated using Equations 6 & 7.

$$\theta_{pixel} = \frac{PixelPitch}{FocalLength} \tag{6}$$

$$t_{signal} = minimum\left(\frac{\theta_{pixel}}{\omega}, t\right) \tag{7}$$

In Equations 6 & 7, θ_{pixel} is the instantaneous FOV which is calculated using a sensor's pixel pitch and focal length. ω is the angular rate of the target & t is the sensor integration time.

With the signal value calculated, the remaining value needed for the SNR is the background noise. Equations 8 & 9 from [6] are used to calculate the background noise.

$$L_b = 5.6 \times 10^{10} \times 10^{-0.4 M_b} \times \left(\frac{180}{\pi}\right)^2 \times 3600^2 \tag{8}$$

$$e_b = Q_e \times \tau \times L_b \times A \times \theta_{pixel}^2 \times t \tag{9}$$

In Equations 8 & 9, L_b is the background signature in $ph/sec/m^3/sr$, M_b is the background visual magnitude per square arcsec. The value of M_b includes sky brightness as well as stray light from any other sources that would impact the analysis, & e_b is the number of background photoelectrons. With the signal and noise functions, the SNR is calculated as per Equation 10.

$$SNR = \frac{e_s}{\sqrt{e_b + e_n^2 + (e_{DC} \times t)}} \tag{10}$$

In calculating the SNR in Equation 10, three sources of noise are considered: the background noise e_b, read noise e_n, and the dark current noise e_{DC}. In [6], dark current is not taken into consideration. We have taken dark current into consideration in this study due to studying a space-based observer, which encounters more extreme temperatures, as opposed to a ground-based observer.

3. RESULTS

This section shows the results of performing the analysis as explained in Section 2. The first step is to propagate the host's (CASSIOPE's) orbit and to generate 100 random co-orbiting objects as per the orbital parameters listed in Table 2. These parameters were varied according to a normal distribution, with the values in Table 2 representing the mean, in the first column, and a 3-sigma variation, in the second column. Out of 100 randomly distributed targets, 13 RSOs have instances where they are within 250 km of the observer with a total of 25 close approaches for a span of 1 day. Fig. 1 shows a semi-log plot of the host to target distance over the 1 day scenario for the 100 generated targets.

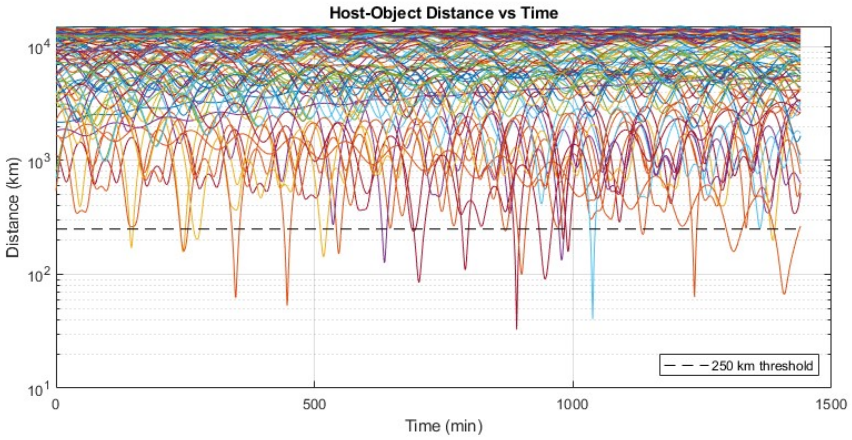

Fig. 1: Plot of host to target distance for 100 randomly generated co-orbiting objects for 1 day.

Fig. 2 shows the location of the close approaching targets with regards to the host's orbit. From Fig. 2, most close approaching targets are near the host orbit's normal or anti-normal vector. If we are planning a mission and deciding on where to aim the sensor to best detect nearby RSOs, in this particular case, aiming it such that the FOV is along the orbit's normal or 180 degrees from the orbit normal vector ensures that most nearby objects would be visible. This is only concerning the geometry of the orbits as we have not yet assessed the detection capabilities of the different sensors.

With the host to target orbits understood, the next part is to determine how well each of our three sensors, the FAI, PCO, & IDS are capable of detecting nearby RSOs. Most sensors allow the user to choose from a range of different integration times. Fig. 3 shows the impact of integration time on the number of detected RSO sequences for each of the three sensors. As noted in Table 3, an RSO is considered to be detected if it is observed with a minimum SNR of 6.

From Fig. 3, we determine that the PCO performs best for detection followed by the FAI and then the IDS camera. For the PCO camera, the number of detected close approaches decreases as the integration time increases with a maximum detection rate for integration times less than or equal 500 milliseconds. For the FAI, the number of detected objects first increases and then decreases with integration time with a maximum detection rate at integration times of 700 - 800 milliseconds. For the IDS camera, the detection rate remains stable until an integration time of about 5.5 seconds where it begins to decrease. The impact of integration time is different for the different sensors due to a combination of two factors. First, an increase in integration time increases the number of received photons in the detector which would increase the SNR but this effect is countered by the fact that the increase in integration time increases the length of the RSO streak. This in turn increases the impact of noise that subsequently reduces the SNR. In most cases, the streaking causes a reduction in the SNR with the exception of FAI for integration times up to 800 milliseconds where the increasing photon count supersedes the impact of the additional noise.

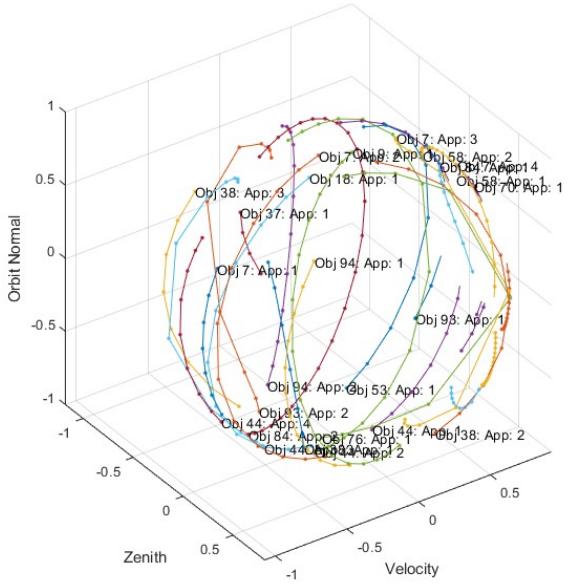

Fig. 2: Location of close approaching targets within the host's orbit.

The last analysis considers the distance, visual magnitude & SNR for the close approaching targets at four points in each sequence: the entry, exit, minimum rate, & minimum distance points. The entry & exit points are studied as they represent the beginning an end of each sequence. The point of minimum angular rate is studied due to the reduced host to target relative motion. This means the target may be detected more easily. Lastly, the minimum distance point is studied as the reduced distance is expected to increase the brightness of the observed target. Table 4 shows the host to target distance for every close approach.

Table 4: Host to target distance.

RSO Number	Approach Number	Host to Target Distance (km)			
		Entry	Exit	Minimum Rate	Minimum Distance
7	1	247.23	248.46	243.02	238.43
7	2	222.66	217.75	222.66	109.80
7	3	217.78	214.04	170.57	32.73
7	4	232.09	233.32	199.34	158.57
9	1	246.41	236.80	246.41	99.69
18	1	242.23	238.92	204.22	132.59
37	1	244.97	245.23	244.97	241.10
38	1	236.46	243.41	206.46	170.65
38	2	243.98	244.44	243.98	156.92
38	3	235.99	241.38	235.99	198.23
44	1	235.29	245.73	223.56	160.64
44	2	223.33	220.87	223.33	62.57
44	3	248.69	228.64	248.69	53.03
44	4	228.52	232.51	201.05	151.34
53	1	233.91	212.12	233.91	126.64
58	1	244.75	243.34	226.31	158.83
58	2	240.43	242.19	240.43	66.91

Table 4 continued from previous page

RSO Number	Approach Number	Host to Target Distance (km)			
		Entry	Exit	Minimum Rate	Minimum Distance
70	1	243.10	241.94	243.10	203.78
76	1	207.45	204.91	207.45	40.38
84	1	245.87	241.16	217.91	84.99
84	2	234.40	231.67	234.40	90.59
93	1	245.77	246.86	245.77	223.53
93	2	209.07	227.95	176.45	63.33
94	1	237.99	240.50	237.99	202.78
94	2	226.53	224.39	226.53	142.89

In Table 4, the first column represents the RSO number out of the 100 propagated orbits. The approach number is a counter for the number of close approaches each target makes. For example, the 7th and 44th RSOs appear within 250 km from the observer a total of 4 times. While the distances at the entry, exit, and minimum rate points are close to 250 km, the minimum distance is typically much smaller. It is as close as 32 km for RSO number 7's third approach. Table 5 shows the value of the visual magnitude for each target's approach at the entry, exit, minimum rate, & minimum distance points.

Table 5: Target visual magnitude.

RSO Number	Approach Number	Visual Magnitude			
		Entry	Exit	Minimum Rate	Minimum Distance
7	1	11.14	11.45	11.56	11.59
7	2	9.05	9.35	9.05	9.37
7	3	8.07	8.25	7.69	3.06
7	4	7.62	7.77	7.29	6.52
9	1	8.24	9.59	8.24	7.18
18	1	11.17	8.35	8.16	8.88
37	1	9.67	8.75	9.67	8.98
38	1	7.61	7.79	7.28	6.65
38	2	8.93	9.18	8.93	8.41
38	3	12.04	10.46	12.04	13.76
44	1	9.33	11.22	11.44	12.11
44	2	8.45	9.66	8.45	9.00
44	3	8.17	8.75	8.17	4.48
44	4	7.57	8.08	7.62	6.58
53	1	12.17	8.44	12.17	10.99
58	1	7.61	9.62	9.23	7.11
58	2	7.76	10.21	7.76	4.73
70	1	7.96	7.45	7.96	7.17
76	1	9.12	7.95	9.12	5.91
84	1	7.75	9.28	8.95	5.41
84	2	8.48	10.61	8.48	9.52
93	1	14.91	10.37	14.91	12.39
93	2	9.19	8.06	7.54	6.03
94	1	9.30	7.72	9.30	7.87
94	2	14.98	7.90	14.98	8.98

From Table 5, most targets are the brightest at the minimum distance point. This does not occur for all approaches though. For example, for the second approach of target RSO number 84, the object appears brightest at the entry point. To determine how well each target's approach is observed from the host RSO, Tables 6 - 8 show the SNR for each target for each sensor at an integration time of 100 milliseconds.

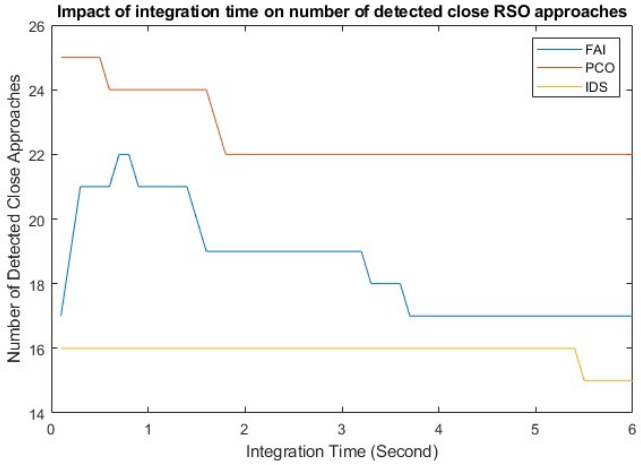

Fig. 3: Impact of integration time on the number of detected close approaches for FAI, PCO, & IDS.

Table 6: Target SNR for FAI.

RSO Number	Approach Number	SNR			
		Entry	Exit	Minimum Rate	Minimum Distance
7	1	0.43	0.32	0.29	0.28
7	2	2.95	2.24	2.95	2.20
7	3	7.29	6.17	10.33	732.92
7	4	11.01	9.61	14.97	30.36
9	1	6.21	1.80	6.21	16.53
18	1	0.42	5.63	6.71	3.47
37	1	1.67	3.91	1.67	3.15
38	1	11.15	9.48	15.13	27.01
38	2	3.31	2.62	3.31	5.35
38	3	0.19	0.81	0.19	0.04
44	1	2.28	0.40	0.33	0.18
44	2	5.12	1.69	5.12	3.09
44	3	6.65	3.88	6.65	199.04
44	4	11.51	7.21	11.05	28.85
53	1	0.17	5.19	0.17	0.50
58	1	11.16	1.75	2.51	17.60
58	2	9.72	1.02	9.72	157.86
70	1	8.05	12.94	8.05	16.71
76	1	2.77	8.15	2.77	53.20
84	1	9.77	2.39	3.24	84.48
84	2	5.01	0.70	5.01	1.92
93	1	0.01	0.88	0.01	0.14
93	2	2.59	7.37	11.90	47.65
94	1	2.35	10.08	2.35	8.76
94	2	0.01	8.51	0.01	3.17

Table 7: Target SNR for PCO.

RSO Number	Approach Number	SNR			
		Entry	Exit	Minimum Rate	Minimum Distance
7	1	10.14	7.84	7.07	6.78
7	2	74.82	56.47	74.82	25.40
7	3	368.27	311.48	521.85	3346.12
7	4	366.80	320.44	498.96	468.30
9	1	224.75	65.06	224.75	216.07
18	1	9.15	123.17	146.82	38.89
37	1	47.50	106.69	47.50	85.94
38	1	272.75	241.29	385.08	394.70
38	2	71.33	53.33	71.33	69.59
38	3	3.70	15.75	3.70	0.63
44	1	55.58	9.97	8.20	3.23
44	2	183.77	57.86	183.77	22.03
44	3	335.73	196.09	335.73	1307.80
44	4	485.55	332.02	509.31	525.67
53	1	3.39	90.53	3.39	4.76
58	1	563.93	88.34	126.65	889.13
58	2	490.85	51.43	490.85	4583.34
70	1	155.72	247.06	155.72	258.68
76	1	88.63	253.14	88.63	227.81
84	1	493.33	120.51	163.46	1466.44
84	2	238.00	28.62	238.00	34.54
93	1	0.25	16.19	0.25	2.38
93	2	97.69	312.93	505.26	311.34
94	1	57.61	242.60	57.61	197.90
94	2	0.36	244.19	0.36	51.81

Table 8: Target SNR for IDS.

RSO Number	Approach Number	SNR			
		Entry	Exit	Minimum Rate	Minimum Distance
7	1	0.39	0.30	0.27	0.26
7	2	2.89	2.18	2.89	0.98
7	3	16.13	13.64	22.85	129.15
7	4	14.16	12.37	19.26	18.07
9	1	8.67	2.51	8.67	8.34
18	1	0.35	4.75	5.67	1.50
37	1	1.83	4.12	1.83	3.32
38	1	10.53	9.31	14.86	15.23
38	2	2.75	2.06	2.75	2.69
38	3	0.14	0.61	0.14	0.02
44	1	2.15	0.38	0.32	0.12
44	2	7.09	2.23	7.09	0.85
44	3	14.70	8.59	14.70	50.48
44	4	18.74	12.81	19.66	20.29
53	1	0.13	3.49	0.13	0.18
58	1	24.69	3.87	5.55	38.93
58	2	21.49	2.25	21.49	176.90

Table 8 continued from previous page

RSO Number	Approach Number	SNR			
		Entry	Exit	Minimum Rate	Minimum Distance
70	1	6.01	9.54	6.01	9.98
76	1	3.42	9.77	3.42	8.79
84	1	21.60	5.28	7.16	56.60
84	2	9.19	1.10	9.19	1.33
93	1	0.01	0.62	0.01	0.09
93	2	3.77	12.08	19.50	12.02
94	1	2.22	9.36	2.22	7.64
94	2	0.01	9.42	0.01	2.00

From Tables 6 - 8, the best SNR results when the PCO camera is used for observation followed by the FAI & IDS cameras. The large aperture and small pixel pitch allows the PCO to detect RSOs with better quality than the other two sensors.

4. CONCLUSIONS

In conclusion, this study presents a pre-mission detectability analysis to allow mission developers to assess the capabilities of different sensors for a particular mission. This analysis studied the orbit of the CASSIOPE satellite to compare the performance of three sensors in detecting small & nearby RSOs. Using the locations of potential close approaches, we determined that aligning the sensor with the orbit normal or anti-normal frame would result in the most detections. When looking at integration times, the PCO camera outperformed the FAI & IDS in the number of detected RSOs. The best performance of the PCO is at integration times below 500 milliseconds. When comparing the SNR of different targets, the PCO camera again outperforms the other two sensors. This analysis can be extended to other missions using the provided equations. Future work includes combining this analysis tool with TLEs of actual targets. At the moment, a series of 100 randomly generated co-orbiting objects was generated. This is to be expanded to add the option for propagating all RSOs with available TLEs to determine which RSOs would truly be co-orbiting to determine how often it happens and if there are any other trends of interest.

5. REFERENCES

[1] Kevin Bernard. Optical co-orbital measurements in low earth orbit. 2019. https://repository.library.carleton.ca/concern/etds/wp988k60n?locale=en.

[2] Randa Qashoa, Matthew Driedger, Ryan Clark, Paul Harrison, Michael Berezin, Regina S. K. Lee, and Andrew Howarth. SPACEDUST-Optical: Wide-FOV Space Situational Awareness from Orbit. In *The Advanced Maui Optical and Space Surveillance Technologies (AMOS) Conference*, 2023. https://amostech.com/TechnicalPapers/2023/Poster/Qashoa2.pdf.

[3] Randa Qashoa, Vithurshan Suthakar, Gabriel Chianelli, Perushan Kunalakantha, and Regina S. K. Lee. Technology demonstration of ssa mission on stratospheric balloon platform. *Remote Sensing*, 16(5):749, 2 2024. https://www.mdpi.com/2072-4292/16/5/749.

[4] Perushan Kunalakantha, Andrea Vallecillo Baires, Siddharth Dave, Ryan Clark, Gabriel Chianelli, and Regina S.K. Lee. Stratospheric Night Sky Imaging Payload for Space Situational Awareness (SSA). *Sensors 2023, Vol. 23, Page 6595*, 23(14):6595, 7 2023. https://www.mdpi.com/1424-8220/23/14/6595/htmhttps://www.mdpi.com/1424-8220/23/14/6595.

[5] William E Krag. Visible magnitude of typical satellites in synchronous orbits. 1974. https://apps.dtic.mil/sti/tr/pdf/AD0785380.pdf.

[6] James R Shell. Optimizing orbital debris monitoring with optical telescopes. In *The Advanced Maui Optical and Space Surveillance (AMOS) Technologies Conference*, 2010. https://amostech.com/TechnicalPapers/2010/Systems/Shell.pdf.